Available online at www.sciencedirect.com

ScienceDirect

materialstoday: PROCEEDINGS

www.materialstoday.com/proceedings

Materials Today: Proceedings 1 (2014) 82 – 93

The 1st International Joint Mini-Symposium on Advanced Coatings between Indiana University-Purdue University Indianapolis and Changwon National University

First principles study on the electrochemical, thermal and mechanical properties of $LiCoO_2$ for thin film rechargeable battery

Linmin Wu, Weng Hoh Lee, Jing Zhang*

Department of Mechanical Engineering, Indiana University-Purdue University Indianapolis, Indianapolis, IN46202, USA

Abstract

Thin film rechargeable battery has become a research hotspot because of its small size and high energy density. Lithium cobalt oxide as a typical cathode material in classical lithium ion batteries is also widely used in thin film rechargeable batteries. In this work, the electrochemical, mechanical and thermal properties of $LiCoO_2$ were systematically investigated using the first principles method. Elastic constants under hydrostatic pressures between 0 to 40 GPa were computed. Specific heat and Debye temperature at low temperature were discussed. Thermal conductivity was obtained using the imposed-flux method. The results show good agreements with experimental data and computational results in literature.

Keywords: $LiCoO_2$; first principles; rechargeable battery; thermal property; mechanical properties; thermodynamic property

* Corresponding author. Tel.: +1-317-278-7186; fax: +1-317-274-9744.
E-mail address: jz29@iupui.edu

doi:10.1016/j.matpr.2014.09.017

1. Introduction

Efficient and durable energy storage is one of the major factors limiting the development of renewable energy. Since lithium-ion batteries were first commercialized by Sony in 1991, they have played a significant role in energy storage devices. Among all of these energy storage devices, one of the promising secondary batteries is thin film rechargeable lithium ion batteries. They are similar to conventional lithium ion batteries, but they are made of thinner materials [1]. Thin film lithium ion batteries are composed of cathode, anode, electrolyte, current collector and separator [1]. Compared to the conventional lithium ion batteries, thin film rechargeable batteries exhibit the same voltage and current, but they have a lighter weight and have a better cycle life due to less polarization. These properties make thin film lithium ion batteries unique to the application of portable electronics and medical devices.

One of the commonly used positive electrode materials in lithium-ion batteries is lithium cobalt oxide ($LiCoO_2$) developed by Goodenough and Mizushima in 1980s [2]. Like conventional lithium ion batteries, $LiCoO_2$ can also be applied to thin film rechargeable lithium ion batteries.

The cathode materials in conventional lithium-ion batteries operate by inserting or extracting lithium ions into and from the host (see Fig.1) [3]. Ordering of lithium and vacancies has a significant effect on the physical and electrochemical properties of the host materials [4]. Due to the excellent electrochemical properties of lithium cobalt oxide, it becomes one of the most widely used cathode materials in lithium-ion batteries. Lithium cobalt oxide consists of layers of lithium that lie between slabs of octahedron formed by cobalt and oxygen atoms [5]. Both lithium and cobalt are octahedrally coordinated by oxygen. The octahedrons are edge-sharing, and tilted relative to the layered structure. The edge-shared octahedral has the properties of direct metal-metal interaction and 90° metal-oxygen-metal interaction. This allows $LiCoO_2$ to have a pretty good ionic and electronic conductivity among ceramic materials. $LiCoO_2$ has a very good electrochemical performance. It can provide a good capacity and high voltage. High capacity and high voltage mean a large maximum theoretical specific energy (MTSE). As shown in Fig.2, the charge-discharge curve of $LiCoO_2$ half cell under 0.4 mA/cm^2 current density showed symmetry, which indicates a good electrochemical performance. In Fig.3, $LiCoO_2$ half cell almost reached the maximum theoretical capacity at 0.2 C rate. And it showed a very good stability of capacity during multiple cycles (see Fig.4).

Batteries produced with $LiCoO_2$ cathodes, while providing good capacity, are more reactive and have worse thermal stability than batteries produced with other cathode materials (eg. $LiFePO_4$ and $LiMnO_2$). This makes $LiCoO_2$ batteries more susceptible to thermal runaway in cases of high temperature operation (>130 °C) or overcharging [6]. At elevated temperatures, $LiCoO_2$ decomposition generates oxygen. Then oxygen reacts exothermically with the organic materials in the cell [6]. This may pose a safety issue due to the highly-exothermic reaction.

Many previous studies focused on the electrochemical and thermal properties of lithium cobalt oxide by experiments. Mizushima and Goodenough [7] first reported the excellent electrochemical properties of $LiCoO_2$. They found $LiCoO_2$ has low overpotential and good reversibility. Reimers et al.[8] studied the electrochemical properties of Li_xCoO_2 by *in situ* X-ray diffraction, and they found the phase transition to the lithium ordered phase near x=1/2 is accompanied by a lattice distortion to a monoclinic unit cell. Yang Shao-horn et al. [9] succeeded to obtain an atomic resolution of $LiCoO_2$ using transmission electron microscope. Kawaji et al. [10] reported the heat capacity and thermodynamic properties of $LiCoO_2$ at low temperatures. There are also many studies on the properties of $LiCoO_2$ by simulation method. Ceder et al.[11] calculated the diffusion coefficient of Li_xCoO_2 using the first principles method. Hart and Bates [12] investigated the strain energy density of $LiCoO_2$ using lattice model.

Although there are many studies on $LiCoO_2$, but atomic scale simulations of the mechanical and thermal properties are rare, especially pressure-dependent bulk modulus, heat capacity and thermal conductivity. This paper will systematically investigate the electrochemical, mechanical and thermal properties of $LiCoO_2$ using the first principles method.

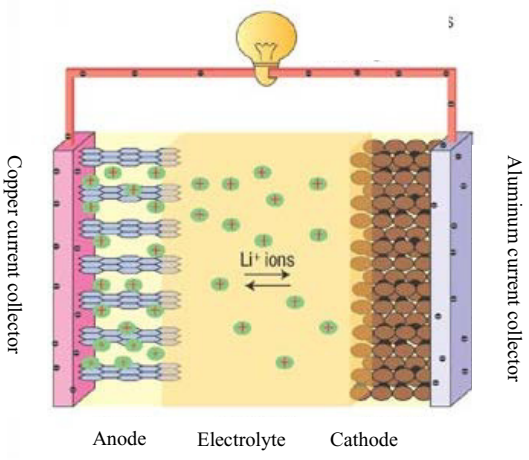

Fig.1 Schematic of lithium-ion batteries [3]

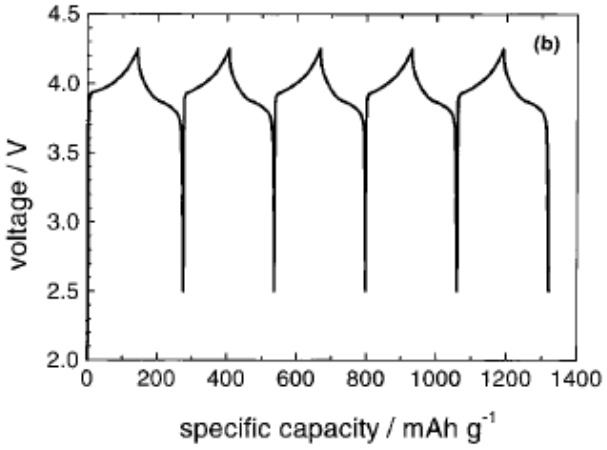

Fig.2 Charge-discharge curve of LiCoO2/Li cells. Current density is 0.4mA/cm^2 [13]

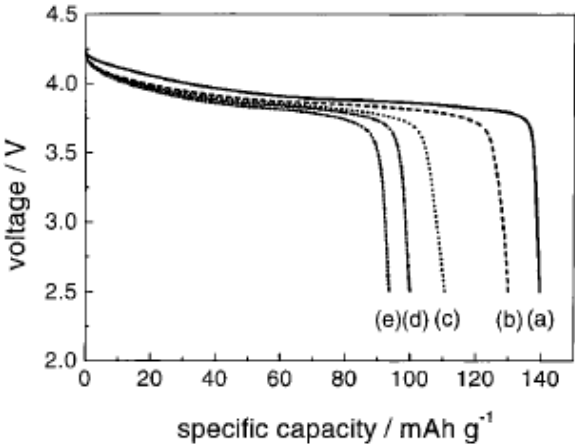

Fig.3 Voltage-specific capacity curve of $LiCoO_2$/Li half cell. (a) 0.2 C rate (b) 0.4 C rate (c) 0.6 C rate (d) 0.8 C rate (e) 1 C rate [13]

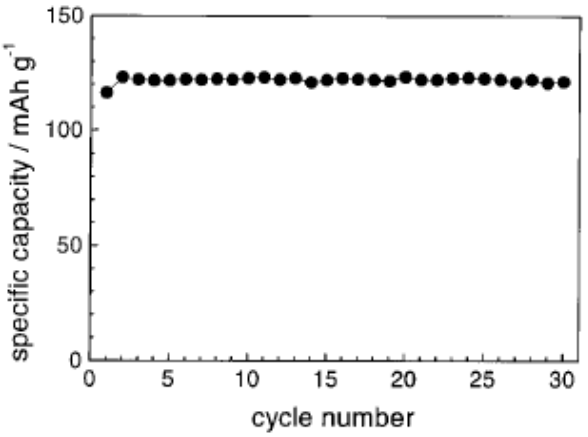

Fig.4 Specific capacity-cycle number curve of $LiCoO_2$/Li half cell at 0.2 C rate [13]

2. Method

For many-body electronic structures, the calculations are very complicated. A stationary electronic state satisfies the many-electron time-dependent Schrödinger equation [14]:

$$H\Psi = \left[T + V + U\right]\Psi = \left[\sum_i^N \left(-\frac{\hbar^2}{-2m_i}\nabla_i^2\right) + \sum_i^N V\left(\vec{r}_i\right) + \sum_{i<j}^N U\left(\vec{r}_i, \vec{r}_j\right)\right]\Psi = E\Psi \qquad (1)$$

where Ψ is the wavefunction, H is the Hamiltonion, T is the kinetic energy, U is the electron-electron interaction energy, V is the potential energy from the external field, $\hbar$ is the Plank constant, E is the total energy, m_i is the

mass of the i_{th} particle, $\vec{r}_i$ is the position vector of the i_{th} particle. It is very difficult to solve the electron-electron interaction term. In density functional theory (DFT), Kohn and Sham simplified the interacting electrons system to a non-interacting electrons system, and developed the Kohn-Sham equation [15]:

$$\left[-\frac{\hbar^2}{2m}\nabla^2 + V_{eff}\left(\vec{r}\right)\right]\phi_i\left(\vec{r}\right) = \varepsilon_i\phi_i\left(\vec{r}\right) \tag{2}$$

where V_{eff} is the local effective potential in which the non-interacting particles move, ε_i is the energy of corresponding Kohn-Sham orbital ϕ_i.

The electrochemical, mechanical and thermal properties were calculated using the DFT method. All calculations in the present study were performed at Generalized Gradient Approximations (GGA) + Perdew Burke Ernzerhof (PBE) [16], and GGA with the projector augmented wave (PAW) method [17], respectively. Here, GGA functionals were selected because they are more reliable than Local Density Approximations (LDA) functionals for predicting transition metal systems [18]. Since d orbital plays an important role in coordinating for transition metals, the U (on-site coulomb term) value for Co-3d is selected to be 4.91eV according to the literature [19].

All calculations were performed with a unit cell containing 3 formula units (3Li, 3Co and 6O), as shown in Fig. 5. The convergence tests of the total energy with respect to the k-points sampling and cut-off energy have been carefully examined, which ensured that the total energy is converged to within 10^{-5} eV per formula unit. The Monkhorst-Pack [20] scheme 3×3×1 k-points mesh was used for the integration in the irreducible Brillouin zone. Energy cut-off for the plane waves was chosen to be 540 eV. Before the calculation, both the lattice parameters and the ionic positions were fully relaxed, and the final forces on all relaxed atoms were less than 0.005 eV/Å.

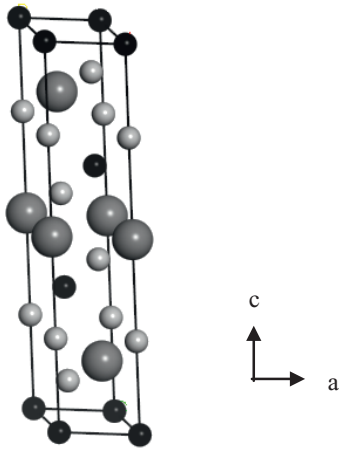

Fig.5 Unit cell of $LiCoO_2$. Black color represents lithium atom, small grey ball represents oxygen atom, large grey ball represents cobalt atom.

3. Results and discussion

$LiCoO_2$ is in $R\bar{3}m$ space group with lattice parameters a=b=2.8156 Å and c=14.0542 Å as reported in [21]. The geometry was optimized using CASTEP and VASP, respectively. From Table 1, the lattice parameters of optimized geometry is consistent with the result in [22]. Further calculations were done based on relaxed unit cell structure.

Table.1 Geometry Optimization of $LiCoO_2$ using CASTEP and VASP

	Before optimization	CASTEP	VASP	Xiong et al (VASP) [22]
a (Å)	2.8156	2.7821	2.8390	2.8369
b (Å)	2.8156	2.7821	2.8390	2.8369
c (Å)	14.0542	13.8415	14.1708	14.1670
A (°)	90	90	90	90
β (°)	90	90	90	90
γ (°)	120	120	120	120

3.1Electrochemical properties

The density of states of $LiCoO_2$ was obtained as shown in Fig.6.

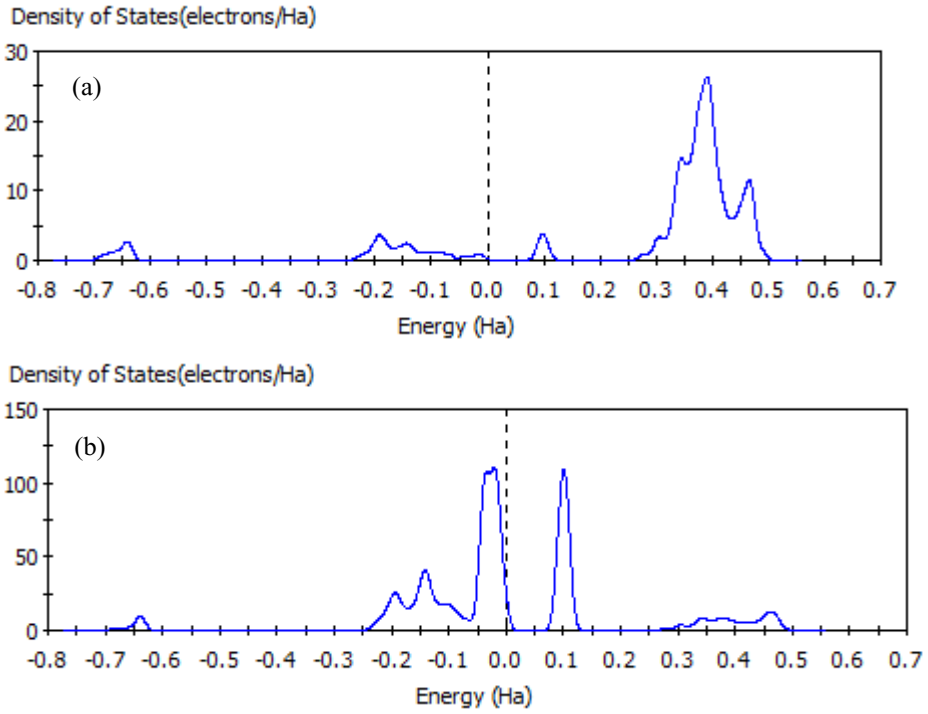

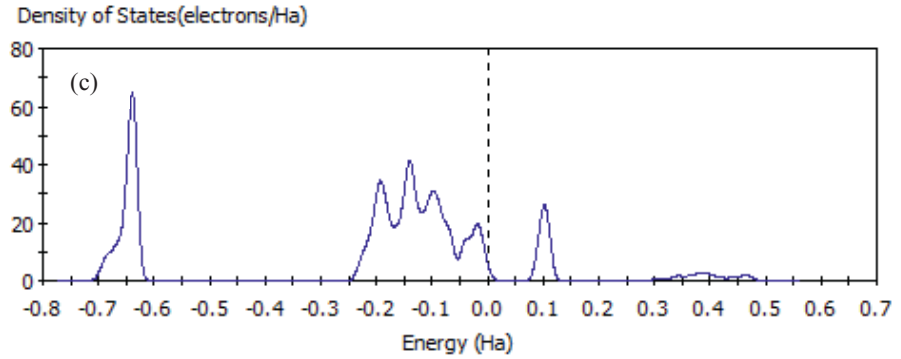

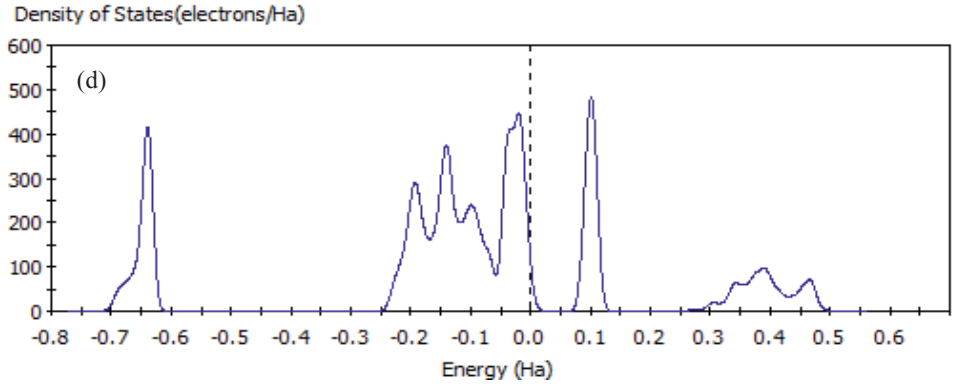

Fig.6 (a) density of states of Li. (b) density of states of Co. (c) density of states of O. (d) density of states of $LiCoO_2$.

The density of states show that the valence band was dominated by O and Co states, while the conduction band was dominated by Li and Co states. The gap is between t_{2g} and e_g Co states slightly hybridized with O 2p states. This is consistent with previous work [23].

The calculated band gap of $LiCoO_2$ in this study was 2.29 eV, which is in good agreement with the experiment result using X-ray photoemmision spectroscopy and bremsstrahlung isochromat spectroscopy [24] and the simulation result [23, 24].

For $LiCoO_2$ material, the reaction of lithium extraction can be expressed as:

$$LiCoO_2 = Li_{1-x}CoO_2 + xLi \tag{3}$$

The average intercalation potential of $LiCoO_2$ is calculated [2] :

$$\Delta G^0 = -nFV \tag{4}$$

Where ΔG^0 is the change of the standard Gibbs free energy, n is number of electrons transferred ($n = 1$ in this study), F is the Faraday constant, V is average lithium extraction potential.

In general, it is assumed that the change in volume and entropy is very small during reaction, so the change of Gibbs free energy can be replaced with the change of internal energy. The structure of $LiCoO_2$ is shown in Fig.5. The structures of Li and CoO_2 are shown in Fig.7. For CoO_2, its space group is $P\bar{3}m1$ with the lattice parameters a=b=2.820 Å and c=4.238 Å as reported [21].

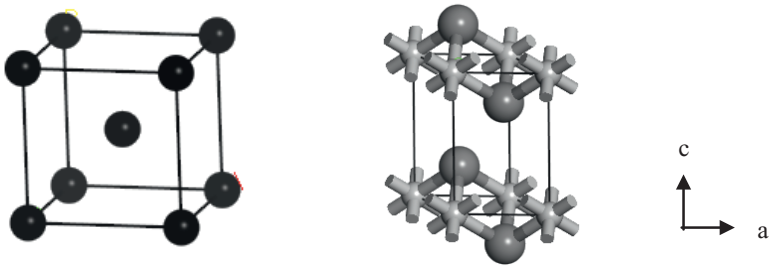

Fig.7 The left figure is the unit cell of Li. The black ball represents lithium atom. The right figure is unit cell of CoO_2. Small grey ball represents cobalt atom, large grey ball represents cobalt atom.

The predicted average intercalation potential calculated using equation (4) was 4.04 V , which is in agreement with the charge/discharge potential plateau of about 4.0 V [25].

3.2 Mechanical properties

The most general relationship which connects stress and strain is the generalized Hook's law [26]:

$$\sigma_{ij} = c_{mnij}\varepsilon_{mn} \tag{5}$$

where σ_{ij} is the stress tensor, ε_{ij} is the strain tensor, and c_{mnij} is the compliance coefficient.

Alternatively, the strains can be described in terms of stresses,

$$\varepsilon_{ij} = S_{mnij}\sigma_{ij} \tag{6}$$

where S_{mnij} is the stiffness coefficient.

Elastic constants and elastic moduli are two fundamental properties providing inner information of the mechanical properties. Since the symmetric nature of the stress and the strain tensor, the 81 coefficients of elastic constants can be reduced to 21 coefficients.

One method to calculate the elastic constants is the stress-strain approach. Once the stress tensor is obtained, elastic constants can be computed according to equation 5 [27].

The computed Young's modulus and bulk modulus are listed in Table.2. From Table.2, the directions (100) and (010) had the same value of the Young's modulus due to the symmetry of the structure. Direction (001) had the smallest value of the Young's modulus. For the Young's modulus, Hart et al. [12] performed the simulation, using the energy-strain approach to calculate the elastic constants. The discrepancy may be caused by different algorithms. In [28], the Young's modulus was measured using nano-indentation experiment. Since the material used in this simulation was single crystal, it is reasonable to get a smaller Young's modulus than the experiment. For bulk modulus, the result is consistent with the previous work [29].

Table.2 Young's modulus and bulk modulus of $LiCoO_2$

	Young's modulus (GPa)	Bulk modulus (GPa)
Hart et al [12]	315-516(Gulp)	
Wang et al [29]		168.5(LDA)
		148.9(GGA)
Qu et al [28]	151-236 (experiment)	
This work	E(001)=E(010)=320.5 E(001)=213.5	171.9 +/- 2.19

Then, we investigated the pressure dependent elastic constants by applying hydrostatic pressures 10, 20, 30 and 40 GPa, respectively.

From Fig.8, we can see the cell volume decreased with the increase of pressure, which follows our instinct. But the slope became smaller with the increase of pressure. The nonlinear increase of atomic forces due to the compression may lead to this phenomenon.

The bulk modulus increased with the increase of pressure (see Fig.9). This can be explained by:

$$Bulk\ \ modulus = -V\frac{dP}{dV} \tag{7}$$

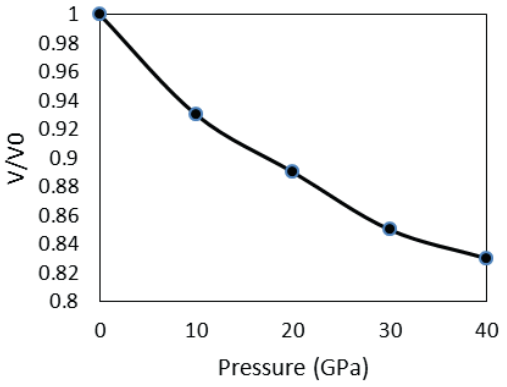

Fig.8 Volume versus pressure curve

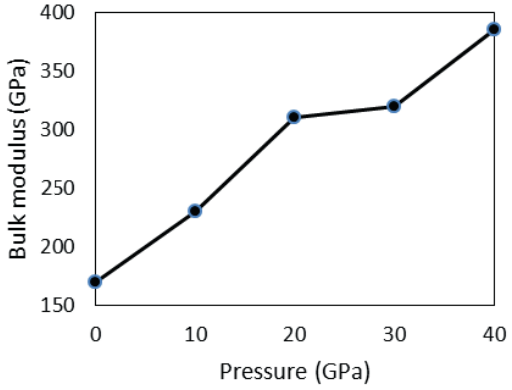

Fig.9 Bulk modulus versus pressure curve

3.3 Thermodynamic properties

When calculating thermal properties, phonon theory should be introduced. Thermodynamic properties are directly related with phonon structures. Once a set of super cells with predefined displacement is built, the forces on atoms of the set of supercells can be computed directly. Thus, mode shapes of phonons can be obtained. Entropy, Holmholtz free energy and heat capacity at constant volume can be derived from quantum mechanics [14]:

$$F = \frac{1}{2}\sum_{q,s}\hbar\omega(q,s) + k_B T\sum_{q,s}\ln\left[1-\exp\left(-\hbar\omega(q,s)/k_B T\right)\right] \tag{8}$$

$$S = -k_B T\sum_{q,s}\ln\left[1-\exp\left(-\frac{\hbar\omega(q,s)}{k_B T}\right)\right] - \frac{1}{T}\sum_{q,s}\frac{\hbar\omega(q,s)}{\exp\left(\frac{\hbar\omega(q,s)}{k_B T}\right)-1} \tag{9}$$

$$C_v = \sum_{q,s}k_B\left[\frac{\hbar\omega(q,s)}{k_B T}\right]^2\frac{\exp\left(\hbar\omega(q,s)/k_B T\right)}{\left[\exp\left(\frac{\hbar\omega(q,s)}{k_B T}\right)-1\right]^2} \tag{10}$$

where F is the Holmholtz free energy, S is entropy, C_V is heat capacity at constant volume, ω is natural frequencies of phonons, $\hbar$ is the Plank constant, k_B is the Boltzman constant and T is temperature.

Gibbs free energy, entropy and enthalpy can be obtained after calculation as shown in Fig.10. Heat capacity at constant volume was compared with the literatures. Kawaji et al [10] , Carlier et al [30] and Maleki et al [31] did experiments on heat capacity measurement. The result of this work shows highly consistency with the literature

(Fig.11).

In Debye theory, the Debye temperature T_D is the temperature of a crystal's highest normal mode of vibration. At low temperatures, the heat capacity at constant volume is proportional to the cube of temperature. And the specific heat at constant volume satisfies the following equation [14]:

$$C_v = 9Nk\left(\frac{T}{T_D}\right)^3 \int_0^{T/T_D} \frac{x^4 e^x}{\left(e^x - 1\right)^2} dx \tag{11}$$

where N is number of atoms, k is the Boltzman constant.

Debye temperature is not a fixed value. It changes with the increase of temperature. The relationship between the Debye temperature and temperature is shown in Fig.12. As temperature increased, the Debye temperature increased at low temperature range 20K to 300K. The simulation result shows a good agreement with the experiment [10]. But the trend of increase slowed down. Because at high temperature, the Debye temperature will become a constant, and the heat capacity at constant volume will reach the Dulong-Petit limit [3].

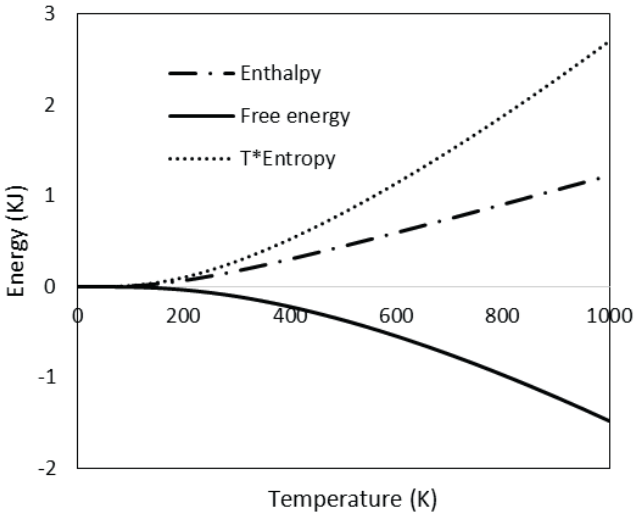

Fig.10 Free energy, enthalpy and entropy of $LiCoO_2$

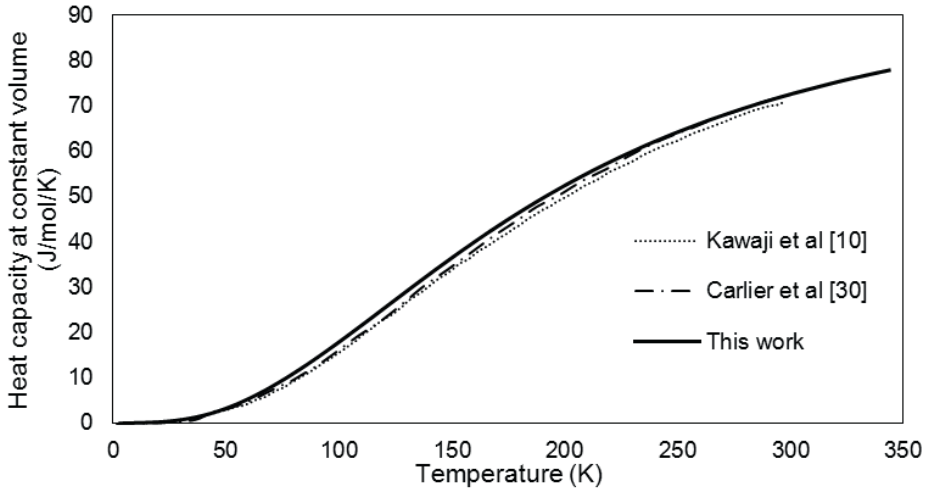

Fig.11 Heat capacity at constant volume of $LiCoO_2$

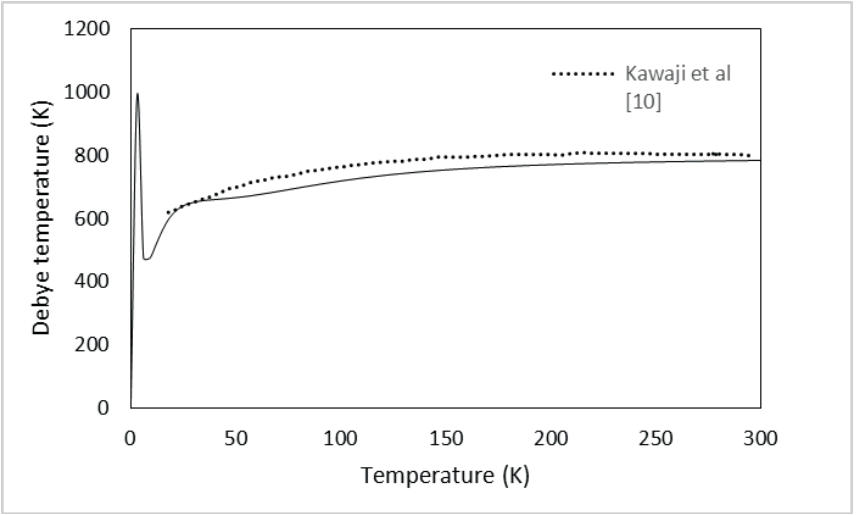

Fig.12 Debye temperature as a function of temperature of $LiCoO_2$

The thermal conductivity of $LiCoO_2$ was calculated using the imposed-flux method [32, 33]. Kinetic energy is exchanged between two fixed layers, repeatedly during a molecular dynamics simulation. Consequently energy flows between the layers. The system responds by creating a temperature gradient. The thermal conductivity follows the Fourier's law [14]:

$$\frac{\Delta Q}{\Delta t} = -K_{th} A \frac{\Delta T}{\Delta x} \tag{12}$$

where $\Delta Q/\Delta t$ is the amount of heat transferred rate, GW; A is the cross section area, m^2; K_{th} is the thermal conductivity, W/m/K; Δx is distance between two ends, m; and $\Delta T/\Delta x$ is temperature gradient along x axis, K/m.

The thermal conductivity was calculated in a one-dimensional model. Thus, a 3×4×20 super cell was built (see Fig.13). The final temperature profile is shown in Fig.14. After the computation, temperature along the super cell and energy flux profile can be obtained (see Fig.15 and Fig.16).

Fig.13 Super cell of $LiCoO_2$

Figure 14 Temperature distribution

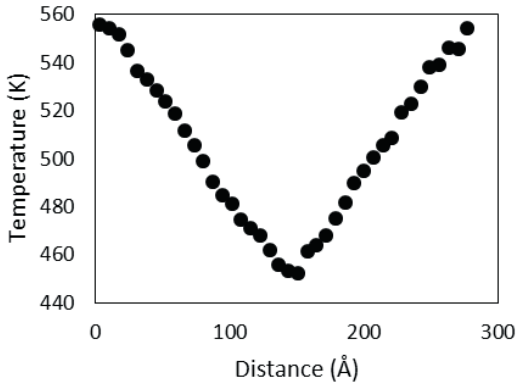

Fig.15 Temperature distribution along c-axis

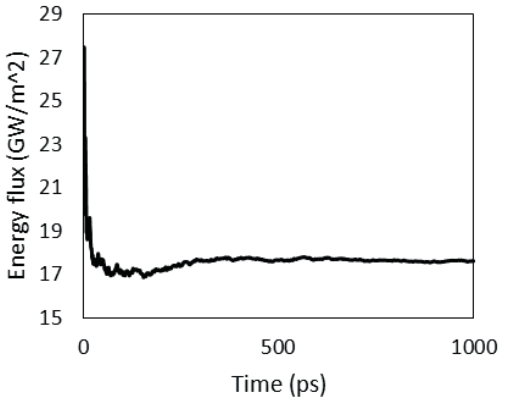

Fig.16 Energy flux time history

From Fig.16, we can see after 400 ps, the energy flux curve became flat, which means the entire system is stable. At 1000 ps, temperature distribution along the c direction of $LiCoO_2$ super cell is plotted in Fig.15. The curve shows the heat flux is in linear relationship with position from high temperature to low temperature, as the temperature gradient in the Fourier's law (eq.12). This result is shown in Fig.14. The calculated temperature gradient was 8.136 GK/m, the energy flux was 17.615 GW/m^2. So thermal conductivity was the ratio of energy flux to temperature gradient, which was 2.165 W/m/K.

In [34], thermal conductivity1.58 W/m/k was obtained by experiment, which was lower than the value of this work, since the sample was a polycrystal. In [35], thermal conductivity 3.7 W/m/K was calculated using molecular dynamics simulation. The difference of value may be caused by different algorithms.

4. Conclusion

In the present study, the electrochemical, mechanical and thermal properties of $LiCoO_2$ were systematically investigated using the first principles method. The result showed the valence band was dominated by O and Co states, while the conduction band was dominated by Li and Co states. The calculated average intercalation voltage of $LiCoO_2$ was 4.04 V. Moreover, the specific heat and Debye temperature calculated is consistent with the literatures. Elastic constants under hydrostatic pressures between 0 to 40 GPa were computed. Bulk modulus increased with the increase of pressure, and cell volume decreased with the increase of pressure. Thermal conductivity was obtained using the imposed-flux method. Calculated thermal conductivity was 2.165 W/m/K, which is consistent with the literature data.

Acknowledgement

J.Z. acknowledges the start-up support provided by the School of Engineering and Technology at Indiana University – Purdue University Indianapolis.

References

[1] L. Hu, H. Wu, F. La Mantia, Y. Yang, and Y. Cui, "Thin, Flexible Secondary Li-Ion Paper Batteries," *ACS Nano,* vol. 4, pp. 5843-5848, 2010/10/26 2010.

[2] T. B. Reddy, "Linden's Handbook of Batteries, 4th edition," *McGraw-Hill,* p. 26.5, 2011.

[3] B. Scrosati, "Nanomaterials: Paper powers battery breakthrough," *Nat Nano,* vol. 3, p. 598, 2007.

[4] Y. Shao-Horn, S. Levasseur, F. Weill, and C. Delmas, "Probing Lithium and Vacancy Ordering in O3 Layered Li_xCoO_2 (x≈0.5) : An Electron Diffraction Study," *Journal of The Electrochemical Society,* vol. 150, pp. A366-A373, March 1, 2003 2003.

[5] I. Nakai, K. Takahashi, Y. Shiraishi, T. Nakagome, F. Izumi, Y. Ishii*, et al.*, "X-ray absorption fine structure and neutron diffraction analyses of de-intercalation behavior in the $LiCoO_2$ and $LiNiO_2$ systems," *Journal of Power Sources,* vol. 68, pp. 536-539, 10// 1997.

[6] D. Doughty and A. Pesaran, "Vehicle Battery Safety Roadmap Guidance," *National Renewable Energy Laboratory,* 2013.

[7] K. Mizushima, P. C. Jones, P. J. Wiseman, and J. B. Goodenough, "Li_xCoO_2 (0<x<1): A new cathode material for batteries of high energy density," *Materials Research Bulletin,* vol. 15, pp. 783-789, 6// 1980.

[8] J. N. Reimers and J. R. Dahn, "Electrochemical and In Situ X-Ray Diffraction Studies of Lithium Intercalation in Li_xCoO_2," *Journal of The Electrochemical Society,* vol. 139, pp. 2091-2097, August 1, 1992 1992.

[9] Y. Shao-Horn, L. Croguennec, C. Delmas, C. Nelson, and M. O'Keefe, " Atomic resolution of lithium ions in $LiCoO_2$," *Nature Material,* vol. 2, p. 464, 2003.

[10] H. Kawaji, M. Takematsu, T. Tojo, T. Atake, A. Hirano, and R. Kanno, "Low temperature heat capacity and thermodynamic functions of $LiCoO_2$," *Journal of Thermal Analysis and Calorimetry,* vol. 68, pp. 833-839, 2002/06/01 2002.

[11] A. Van der Ven and G. Ceder, "Lithium Diffusion in Layered Li_xCoO_2," *Electrochemical and Solid-State Letters,* vol. 3, pp. 301-304, July 1, 2000 2000.

[12] F. X. Hart and J. B. Bates, "Lattice model calculation of the strain energy density and other properties of crystalline $LiCoO_2$," *Journal of Applied Physics,* vol. 83, pp. 7560-7566, 1998.

[13] B. Huang, Y. I. Jang, Y. M. Chiang, and D. R. Sadoway, "Electrochemical evaluation of $LiCoO_2$ synthesized by decomposition and intercalation of hydroxides for lithium-ion battery applications," *Journal of Applied Electrochemistry,* vol. 28, pp. 1365-1369, 1998/12/01 1998.

[14] N. W. Ashcroft and N. D. Mermin, "Solid State Physics," *Holt Rinehart & Winston,* 1976.

[15] W. Kohn and L. J. Sham, "Self-Consistent Equations Including Exchange and Correlation Effects," *Physical Review,* vol. 140, pp. A1133-A1138, 11/15/ 1965.

[16] M. D. Segall, P. J. Lindan, M. J. Probert, C. J. Pickard, P. J. Hasnip, S. J. Clark*, et al.*, "First-principles simulation: ideas, illustrations and the CASTEP code," *Journal of Physics: Condensed Matter,* vol. 14, p. 2717, 2002.

[17] G. Kresse and J. Furthmüller, "Efficient iterative schemes for ab initio total-energy calculations using a plane-wave basis set," *Physical Review B,* vol. 54, pp. 11169-11186, 10/15/ 1996.

[18] T. J. Giese and D. M. York, "Density-functional expansion methods: Evaluation of LDA, GGA, and meta-GGA functionals and different integral approximations," *The Journal of Chemical Physics,* vol. 133, pp. -, 2010.

[19] F. Zhou, M. Cococcioni, C. A. Marianetti, D. Morgan, and G. Ceder, "First-principles prediction of redox potentials in transition-metal compounds with LDA+U," *Physical Review B,* vol. 70, p. 235121, 12/20/ 2004.

[20] H. J. Monkhorst and J. D. Pack, "Special points for Brillouin-zone integrations," *Physical Review B,* vol. 13, pp. 5188-5192, 06/15/ 1976.

[21] T. Motohashi, Y. Katsumata, T. Ono, R. Kanno, M. Karppinen, and H. Yamauchi, "Synthesis and Properties of CoO_2, the x = 0 End Member of the Li_xCoO_2 and Na_xCoO_2 Systems," *Chemistry of Materials,* vol. 19, pp. 5063-5066, 2007/10/01 2007.

[22] F. Xiong, H. J. Yan, Y. Chen, B. Xu, J. X. Le, and C. Y. Ouyang, "The Atomic and Electronic Structure Changes Upon Delithiation of $LiCoO_2$: From First Principles Calculations," *International Journal of Electrochemical Science,* vol. 7, p. 9390, 2012.

[23] A. Juhin, F. de Groot, G. Vankó, M. Calandra, and C. Brouder, "Angular dependence of core hole screening in $LiCoO_2$: A DFT+U calculation of the oxygen and cobalt K-edge x-ray absorption spectra," *Physical Review B,* vol. 81, p. 115115, 03/10/ 2010.

[24] J. van Elp, J. L. Wieland, H. Eskes, P. Kuiper, G. A. Sawatzky, F. M. F. de Groot*, et al.*, "Electronic structure of CoO, Li-doped CoO, and $LiCoO_2$," *Physical Review B,* vol. 44, pp. 6090-6103, 09/15/ 1991.

[25] L. Liu, L. Chen, X. Huang, X.-Q. Yang, W.-S. Yoon, H. S. Lee*, et al.*, "Electrochemical and In Situ Synchrotron XRD Studies on Al_2O_3-Coated $LiCoO_2$ Cathode Material," *Journal of The Electrochemical Society,* vol. 151, pp. A1344-A1351, September 1, 2004 2004.

[26] A. C. Ugural and S. K. Fenster, "Advance Mechanics of materials and applied elasticity (5th edition)," *Prentice Hall,* 2011.

[27] Y. Le Page and P. Saxe, "Symmetry-general least-squares extraction of elastic data for strained materials from ab initio calculations of stress," *Physical Review B,* vol. 65, p. 104104, 2002.

[28] M. Qu, W. H. Woodford, J. M. Maloney, W. C. Carter, Y.-M. Chiang, and K. J. Van Vliet, "Nanomechanical Quantification of Elastic, Plastic, and Fracture Properties of $LiCoO_2$," *Advanced Energy Materials,* vol. 2, pp. 940-944, 2012.

[29] H. Wang, Y. I. Jang, B. Huang, D. R. Sadoway, and Y. M. Chiang, "TEM Study of Electrochemical Cycling-Induced Damage and Disorder in $LiCoO_2$ Cathodes for Rechargeable Lithium Batteries," *Journal of The Electrochemical Society,* vol. 146, pp. 473-480, February 1, 1999 1999.

[30] M. Ménétrier, D. Carlier, M. Blangero, and C. Delmas, "On “Really” Stoichiometric $LiCoO_2$," *Electrochemical and Solid-State Letters,* vol. 11, pp. A179-A182, November 1, 2008 2008.

[31] H. Maleki, S. A. Hallaj, J. R. Selman, R. B. Dinwiddie, and H. Wang, "Thermal Properties of Lithium-Ion Battery and Components," *Journal of The Electrochemical Society,* vol. 146, pp. 947-954, March 1, 1999 1999.

[32] P. Jund and R. Jullien, "Molecular-dynamics calculation of the thermal conductivity of vitreous silica," *Physical Review B,* vol. 59, pp. 13707-13711, 06/01/ 1999.

[33] F. Müller-Plathe, "A simple nonequilibrium molecular dynamics method for calculating the thermal conductivity," *The Journal of Chemical Physics,* vol. 106, pp. 6082-6085, 1997.

[34] S.C.Chen, C.C.Wan, and Y.Y.Wang, "Thermal analysis of lithium-ion batteries," *Journal of Power Sources,* vol. 140, pp. 111-124, 2005.

[35] K. Takahata and I. Terasaki, "Thermal Conductivity of A_xBO_2 -type Layered Oxides $Na_{0.77}MnO_2$ and $LiCoO_2$," *Japanese Journal of Applied Physics,* vol. 41, p. 763, 2002.